A tale of two polyamides: comparing the crystallization kinetics of a hot-melt adhesive and a PA 6/66 copolymer

Masoumeh Pourali and Amy M. Peterson*
University of Massachusetts Lowell, Department of Plastics Engineering, Lowell, MA, United States
*Corresponding Author
Email Address: Amy_Peterson@uml.edu

Abstract

In this work, the isothermal and non-isothermal crystallization kinetics of two polyamides, a polyamide-based hot melt adhesive with the trade name of Technomelt PA 6910 and a copolymer of PA 6 and PA 66, are studied using Fast Scanning Calorimetry (FSC) and Differential Scanning Calorimetry (DSC). While both of these materials exhibit good performance as feedstocks for material extrusion additive manufacturing, their crystallization behavior and kinetics differ substantially. Technomelt PA 6910 crystallizes much slower than the PA 6/66 due to the lower density of hydrogen bonding within Technomelt PA 6910's structure. This low hydrogen bonding also results in a low glass transition temperature (T_g), low viscosity, and high flexibility of Technomelt PA 6910 at room temperature. The low T_g encourages room temperature crystallization of Technomelt PA 6910. PA 6/66 is a random copolymer whose faster crystallization is attributed to the high density of hydrogen bonding accompanied by a sheet-like structure of the hydrogen bonding within the melt, which favors high-temperature crystallization. The kinetic results from this study enable coupling the crystallization kinetics of these materials with thermal models for processing techniques including material extrusion additive manufacturing.

Keywords

Crystallization kinetics; Fast scanning calorimetry; Polyamides; Hot melt adhesives

Introduction

Semicrystalline thermoplastics are interesting materials in engineering applications due to their high mechanical strength and excellent heat, chemical, and abrasion resistance [1,2]. However, their crystallization during processing can result in significant shrinkage and warpage due to the different amounts of volumetric contraction in amorphous and crystalline regions. The difference in the volume change of phases can result in thermomechanical stresses and warpage within a part [3–9]. Therefore, assessing the crystallization kinetics of plastics is helpful to understanding and controlling the uniformity of microstructure within a part as well as its shrinkage and warpage during processing.

Prior studies of crystallization have primarily been performed by DSC analysis. Kinetic analysis at low temperatures requires fast cooling to the desired temperature to avoid nuclei formation and growth. However, the scanning rates in DSC are well below 1.5 K/s, which prevents kinetic studies at temperatures approaching the glass transition temperature (T_g) [10–13]. Recently, the development of Flash DSC, a commercial Fast Scanning Calorimeter (FSC), with scan rates as high as 30,000 K/s has enabled kinetic analysis at a wide range of temperatures [14].

As important semicrystalline engineering polymers, there has been a lot of research focus on the crystallization kinetics of polyamides (PAs). The most common PAs have a linear structure with recurring amide groups, which participate in hydrogen bonding within the polymeric chain – these PAs are commonly known as nylons [15,16]. These materials offer high mechanical properties and good chemical and thermal resistance [17–19].

Controlling the crystallization and shrinkage of PAs broadens their applications by making them processable with different techniques. Blending with amorphous polymers, copolymerizing, or compounding with fillers are the most common strategies to control crystallization and warpage of semicrystalline polymers including PAs [2–4,20–22]. For example, Jia et al. controlled the warpage of PA 6 parts manufactured by Fused Filament Fabrication (FFF), a thermally driven form of material extrusion additive manufacturing in which filament is fed into an extruder and selectively dispensed from the extruder as it rasters across a build surface. They achieved this control by blending the PA 6 with a polyolefin elastomer and polystyrene (PS). Blending hindered the regular arrangement of molecular chains of PA 6, which resulted in formation of poorly packed crystallites [4].

In this work, we compare the kinetics of crystallization of two polyamides that are relevant to material extrusion additive manufacturing: a PA 6/66 copolymer and a polyamide-based hot melt adhesive with the trade name of Technomelt PA 6910. This research is motivated in part by our previous work [23], wherein we successfully printed void-free parts with isotropic mechanical properties out of Technomelt PA 6910 using FFF. Slow crystallization down to room temperature was identified as a critical reason mechanical properties comparable or superior to those of compression molded parts could be achieved. To obtain a fundamental understanding of the crystallization behavior of this material, the kinetics of crystallization of Technomelt PA 6910 were studied and compared to a 3D printable polyamide copolymer, PA 6/66.

PA 6/66 crystallization kinetics was previously investigated under isothermal conditions using DSC analysis and these results showed that copolymerization results in slower

crystallization [2]. However, that analysis was limited to high temperatures (i.e, close to the material's melting temperature, T_m) due to the relatively low scan rate achievable with DSC. Recently, Wang et al. investigated the crystallization kinetics of PA 6/66 at a wide range of temperatures using FSC. Their work focused on defining half-time crystallization and does not fit the data to kinetic models [24]. To our best knowledge, there is no reported information about the crystallization behavior of Technomelt PA 6910. Therefore, we investigated the crystallization behavior of these two materials in isothermal and non-isothermal conditions at a wide range of temperatures and scanning rates using DSC and FSC. The data were fit to kinetic models to define the kinetic constants, and the crystallization behavior of these two printable polyamides were compared.

Theory

The Avrami equation is commonly used in studying the kinetics of primary crystallization of materials. This approach considers the crystallization of materials at isothermal conditions. The Avrami equation (Eq. 1) describes the relative crystallinity x(t) at time t, in which k_{Av} is the Avrami kinetic constant, and n is the Avrami exponent [25–27].

$$x(t) = 1 - \exp(-k(t)_{Av} t^n) \qquad \text{Eq. 1}$$

The n value, as defined in Eq. 2, is associated with spherulite nucleation (n_n) and growth (n_g). The n_n value is zero at low temperatures when there is instantaneous or heterogeneous nucleation, and it is equal to 1 when the nucleation is sporadic or homogeneous at high temperatures. The value of n_g varies between 1 and 3 and corresponds to the dimensionality of crystal growth. Therefore, n values range from 1 to 4 based on the mechanisms of nucleation and growth [28].

$$n = n_n + n_g \quad \text{Eq. 2}$$

To make the Avrami model applicable for non-isothermal crystallization process, Jaziorny modified k_{Av} with the cooling rate r as shown in Eq. 3:

$$\mathrm{Log\ k_J} = \frac{\mathrm{Log\ k_{Av}}}{\mathrm{r}} \quad \text{Eq. 3}$$

k_J is the kinetic constant of the Jaziorny model. This model assumes a constant cooling rate and crystallization temperature [29]. However, this approach overpredicts values for the Avrami exponent n, which limits its utility [30].

Ozawa extended the Avrami theory to non-isothermal conditions in which crystallization occurs at constant cooling rates. The Ozawa equation (Eq. 4) describes x(T), where k_{Oz} is the Ozawa rate constant and m is the Ozawa exponent. The value of m depends on the dimension of the crystal growth [31].

$$x(T) = 1 - \exp(-\frac{k(T)_{Oz}}{r^m}) \quad \text{Eq. 4}$$

The Avrami theory was further extended by Nakamura (Eq. 5), defining x(t) as a function of the thermal history T(t) [32].

$$x(t) = 1 - \exp[-\{\int_0^t K\big(T(t)\big)dt\}^n \quad \text{Eq. 5}$$

K is the Nakamura rate constant, which is related to k_{Av} and k_{Oz} by Eq. 6:

$$K = k_{Av}^{\frac{1}{n}} = -\frac{d(k_{Oz}^{\frac{1}{n}})}{dT} \quad \text{Eq. 6}$$

This theory describes the kinetics of non-isothermal crystallization at a non-constant cooling rate, which makes it suitable to predict crystallization during plastic processing. Nakamura's theory was simplified by Patel and Spruiell [33] into its differential form (Eq. 7), which is useful for coupling with thermal models [12].

$$\frac{dx}{dt} = nK(T(t))(1-x)(-Ln(1-x))^{\frac{1}{n}-1} \quad \text{Eq. 7}$$

Materials

Two types of polyamide-based thermoplastics were used in this study. The first is Technomelt PA 6910, a polyamide-based hot melt adhesive, which was kindly provided by Henkel Corporation in the form of strand cut pellets. Detailed characterization of Technomelt PA 6910 is provided in our previous work [23]. The second material used in this study is a natural colored Nylon 6/66 copolymer filament (KODAK 3D Printing Filaments) with a 1.75 mm diameter. KODAK sells this product as their Nylon 6 filament, but it is a copolymer of Nylon 6 and Nylon 66. For consistency, we will refer to the KODAK Nylon 6 product as PA 6/66.

Fast scanning calorimetry (FSC)

FSC was performed with a Mettler-Toledo Flash DSC 2 equipped with a Huber TC-100 intercooler. Experiments were performed within the temperature range of -40 °C to 270 °C, and maximum cooling and heating rates of 1,000 K/s. For sample preparation, an extruded strand from a FFF printer with a diameter of 0.4 mm was used. A thin film was cut from the strand cross-section and was further cut into dust-sized pieces using a scalpel. The prepared sample was transferred to the center area of the UFS1 chip sensor with the help of a strand of hair. Conditioning and correction of the chip sensor were performed before placing the sample on the

sensor based on the standard protocol provided by the manufacturer. To ensure good thermal contact between the sample and sensor, the specimen was pre-melted by slowly heating above its T_m under nitrogen flow at 80 mL/min.

After sample preparation and pre-melting, two experimental procedures were followed. In the first procedure, different cooling rates were used to determine the critical cooling rate to suppress crystallization from the melt as well as to identify changes in melting enthalpy (ΔH_m), T_m, and T_g at different cooling rates. A schematic of this procedure can be seen in Fig. 1a. The first step is heating the material above its T_m for 0.25 s to erase its thermal history, followed by cooling at different rates to allow for melt crystallization. Then, the specimen is heated to evaluate the ΔH_m as a result of melt crystallization. The heating rate was sufficiently high (1,000 K/s) to prevent further crystallization.

The second experimental procedure used isothermal crystallization at different times and temperatures to characterize crystallization kinetics for the two materials. A schematic of this procedure can be seen in Fig. 1b. In this experiment, after erasing the thermal history of the material, it was cooled to the annealing temperature. Annealing was performed at different temperatures and times. After annealing, the specimen was cooled below its T_g to stop crystallization, followed by a heating cycle to evaluate the ΔH_m as a result of crystallization during the annealing step. The heating and cooling steps were sufficiently fast (1,000 K/s) to suppress crystallization before and after the annealing step.

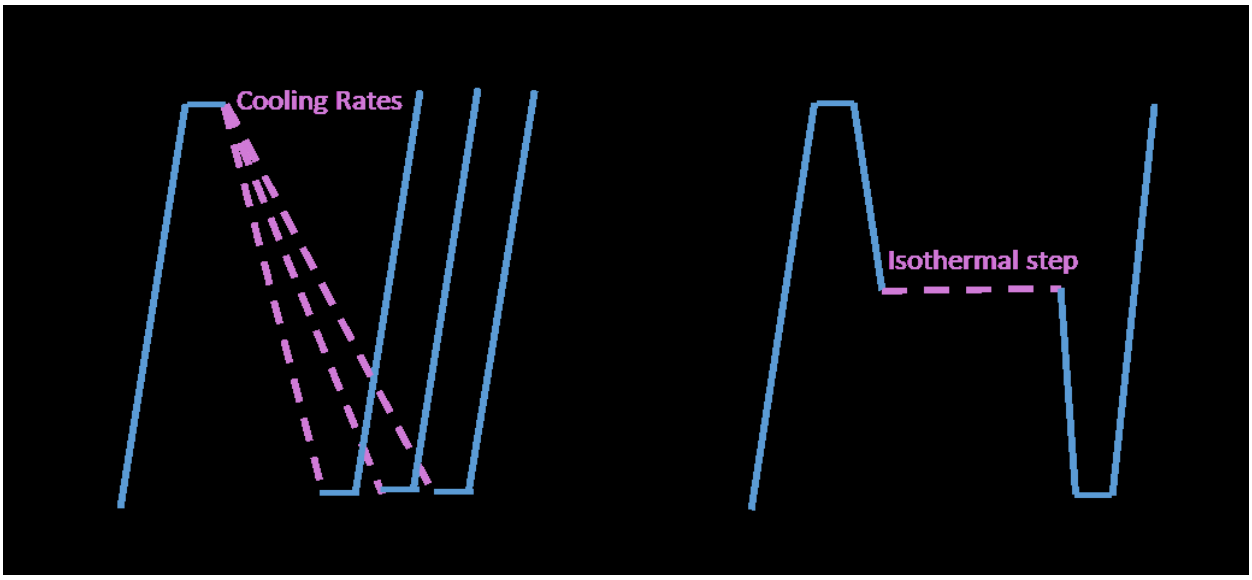

Figure 1. Temperature program for a. melt crystallization; b. isothermal crystallization analyses using FSC.

Differential Scanning Calorimetry (DSC)

The minimum cooling rate at which FSC can be used to realize the heat flow is 0.1 K/s. Therefore, DSC was used for lower cooling rates. DSC was conducted using a Discovery DSC (TA Instruments, USA). DSC samples were prepared in aluminum hermetic pans. Samples were analyzed by a heat-cool-heat cycle with cooling rates ranging from 0.08 K/s (5 K/min) up to 0.28 K/s (17 K/min) to assess the effect of cooling rates on crystallinity.

Results and Discussion

Critical cooling and heating rates

To define the kinetics of isothermal crystallization, it is crucial to suppress melt crystallization while cooling the sample to the isothermal annealing temperature. Therefore, we need to determine cooling rates that are sufficiently fast so as to suppress melt crystallization according to the temperature program in Fig. 1a. The first step is erasing the thermal history by heating the

PA 6/66 and Technomelt PA 6910 for 0.2 s at 260 °C and 150 °C, respectively. After erasing the thermal history, the samples were cooled at rates ranging from 0.2 K/s to 1,000 K/s to temperatures below their T_g, followed by subsequent heating above their T_m at a rate of 1,000 K/s. The FSC results from the 2nd heating cycle in Fig. 2 indicate that cooling rates higher than 2 K/s suppress melt crystallization of Technomelt PA 6910, while cooling rates above 20 K/s suppress melt crystallization of PA 6/66. A relaxation due to physical aging is observed above the T_g of both polyamides at lower cooling rates. The enthalpy of relaxation is noticeable up to the cooling rates of 50 K/s and 20 K/s for Technomelt PA 6910 and PA 6/66, respectively. During aging, ordered molecules can act as nuclei and accelerate future crystallization [34]. Therefore, a cooling rate of 1,000 K/s was used for both materials in subsequent experiments to suppress nucleation and physical aging, and to account for the sensitivity of the FSC in capturing small heat flows.

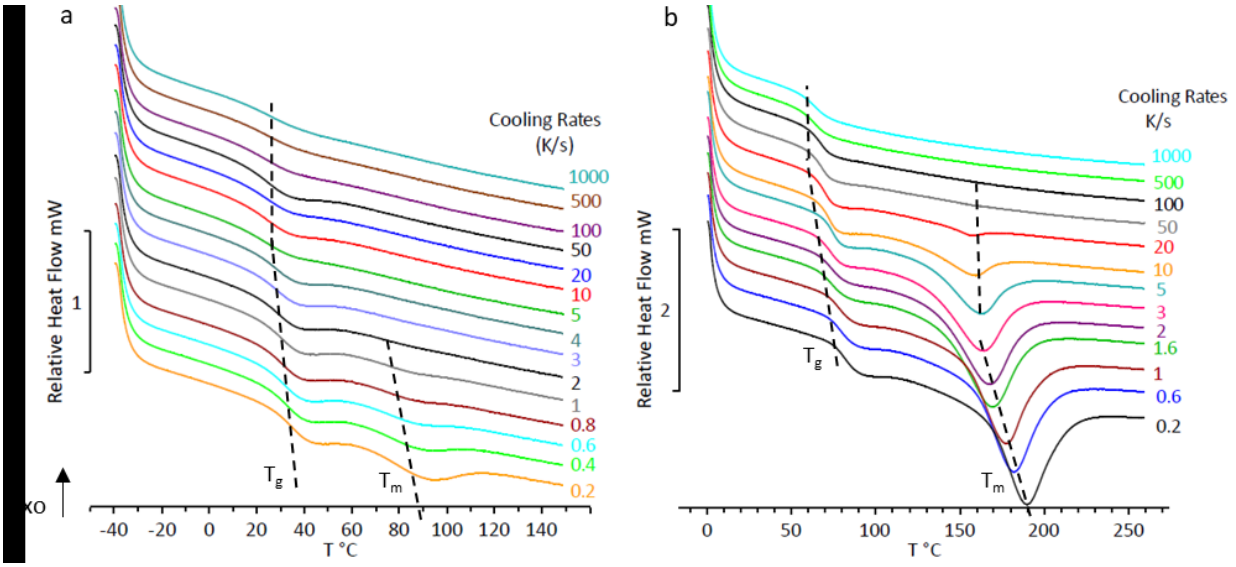

Figure 2. Relative heat flow as a function of temperature in the subsequent heating cycle after cooling at different rates for a. Technomelt PA 6910; b. PA6/66. Dashed lines are used to indicate the locations of the glass transitions and melts.

The effect of heating rate was investigated similarly and no cold crystallization was observed at heating rates as low as 100 K/s after a fast cooling as shown in Fig SI. 1. These results are similar to those of Wang et al., whom reported effective suppression of cold crystallization of PA 6 and PA 66 copolymer at a heating rate of 80 K/s [24]. To account for the sensitivity of FSC in capturing small heat flows, a heating rate of 1,000 K/s was used for all experiments.

Nonisothermal Analysis

As shown in Fig. 2, the thermal properties of both polyamides vary with cooling rate. Therefore, the T_g, T_m, and ΔH_m of the materials as a function of cooling rates are plotted in Fig. 3 for further discussion. From Fig. 3a, the T_g of PA 6/66 and Technomelt PA 6910 decrease with increasing cooling rate. The decrease in T_g is attributed to the ratio of rigid amorphous fraction

(RAF) to the mobile amorphous fraction (MAF) within the structure. The amorphous fraction between the lamellae behaves differently than the bulk amorphous phase in terms of its mobility. RAF is the amorphous fraction coming out of the lamella and exhibits lower mobility. The remaining amorphous fraction with higher mobility is the MAF fraction. A higher ratio of RAF/MAF results in a higher T_g [35,36]. As seen in Fig. 3b and c, T_m and ΔH_m are larger at low cooling rates due to the longer time provided for the movement of molecules and their packing into crystallites before cooling below T_g. The majority of the crystallites formed during cooling are unstable γ-phases. Later, it will be shown that these findings are consistent with isothermal analysis, in which α-phase formation is only favored for isothermal annealing at high temperatures or when annealing for a long time. The RAF increases with an increased fraction of γ-phase and results in higher T_g values at lower cooling rates. These results are also in agreement with the results from Kolesov et al., which showed that the RAF fraction increases with increasing fraction of mesophase crystallites [35]. T_g decreases significantly until reaching a critical cooling rate (100 K/s and 500 K/s for Technomelt PA 6910 and PA 6/66, respectively). Below the critical cooling rate, ordering of molecules can occur, which restricts easy movement of molecules and results in higher T_g. At higher cooling rates the material is fully amorphous with a relatively constant T_g. The heat flow from the ordering of molecules was too small to be detected by FSC at the cooling rates of 2-100 K/s and 20-500 K/s for Technomelt PA 6910 and PA 6/66, respectively. However, ordered molecules can act as nucleating agents and accelerate crystallization at the next heating cycle or annealing step, and their effect needs to be considered in defining the critical cooling rate. The selected critical cooling rate of 1,000 K/s meets these criteria.

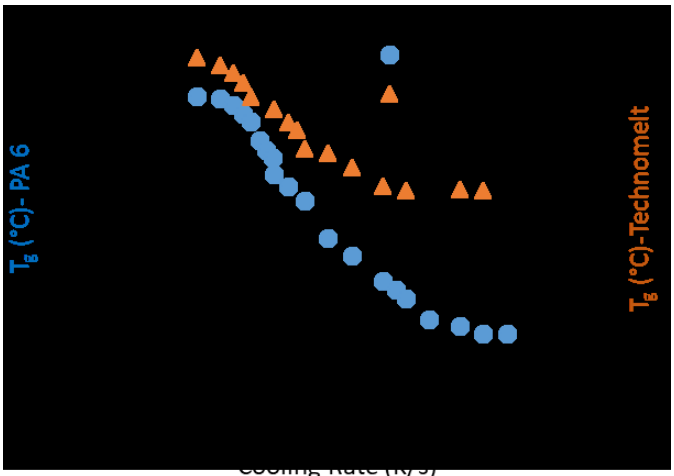

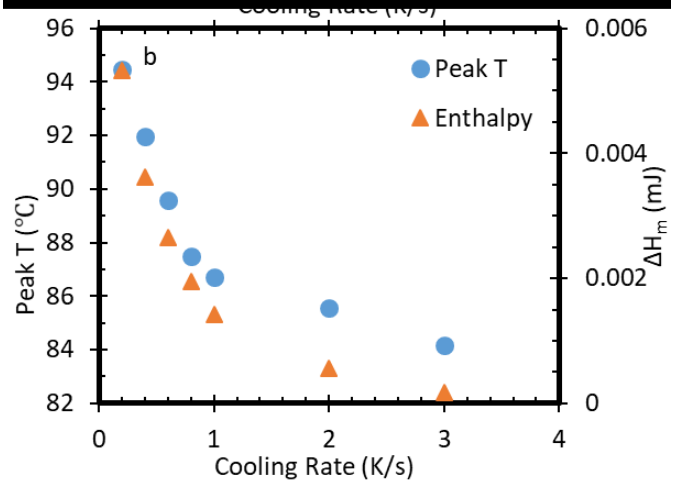

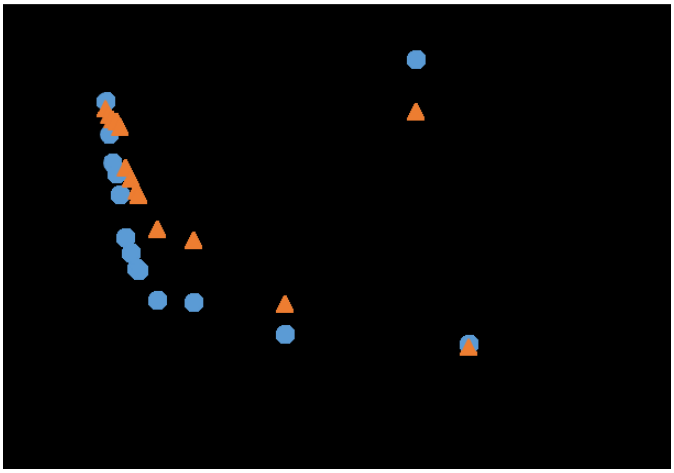

Figure 3. a. T_g of Technomelt PA 6910 and PA 6/66 as a function of cooling rate; b. T_m and ΔH_m of Technomelt PA 6910 as a function of cooling rate obtained from the subsequent heating cycle after melt crystallization at different cooling rates by FSC.; c. T_m and ΔH_m of PA 6/66 as a function of cooling rates obtained from the subsequent heating cycle after melt crystallization at different cooling rates by FSC.

The T_g values obtained for both polyamides from FSC analysis are roughly 35 °C larger than those from DSC analysis of the heating cycle following cooling at a rate of 0.2 K/s (Fig SI. 2). The higher heating rates used in FSC analysis cause the shift in T_g to higher temperatures. The effect of thermal lag is negligible in FSC up to a scan rate of 1,000 K/s [37], so the change in T_g is due to the kinetic nature of the glass transition. At high heating rates, structural relaxation during the glass transition cannot keep up with the high rates of temperature change, and the T_g shifts to higher values [38,39]. A heating rate of 1,000 K/s is used in FSC analysis, which is about 3.7 orders of magnitude larger than the heating rate of 0.2 K/s used in DSC analysis. Increasing the heating rate by one order of magnitude results in about 9 °C increase in the T_g. Previously, one order of magnitude increase in the cooling rate was reported to increase the T_g of Polystyrene (PS) by 3.5 °C [40].

Ozawa's Model:

Fig. 4 shows the percent crystallization of Technomelt PA 6910 and PA 6/66 as a function of time and temperature. For both Technomelt PA 6910 and PA 6/66, decreasing the cooling rate results in a shift of crystallization to higher temperatures. The incubation time for crystallization at a constant cooling rate is significantly longer for Technomelt PA 6910. For example, at the cooling rate of 0.08 K/s, the incubation time for Technomelt PA 6910 is 250 s, while it is only 100 s for PA 6/66.

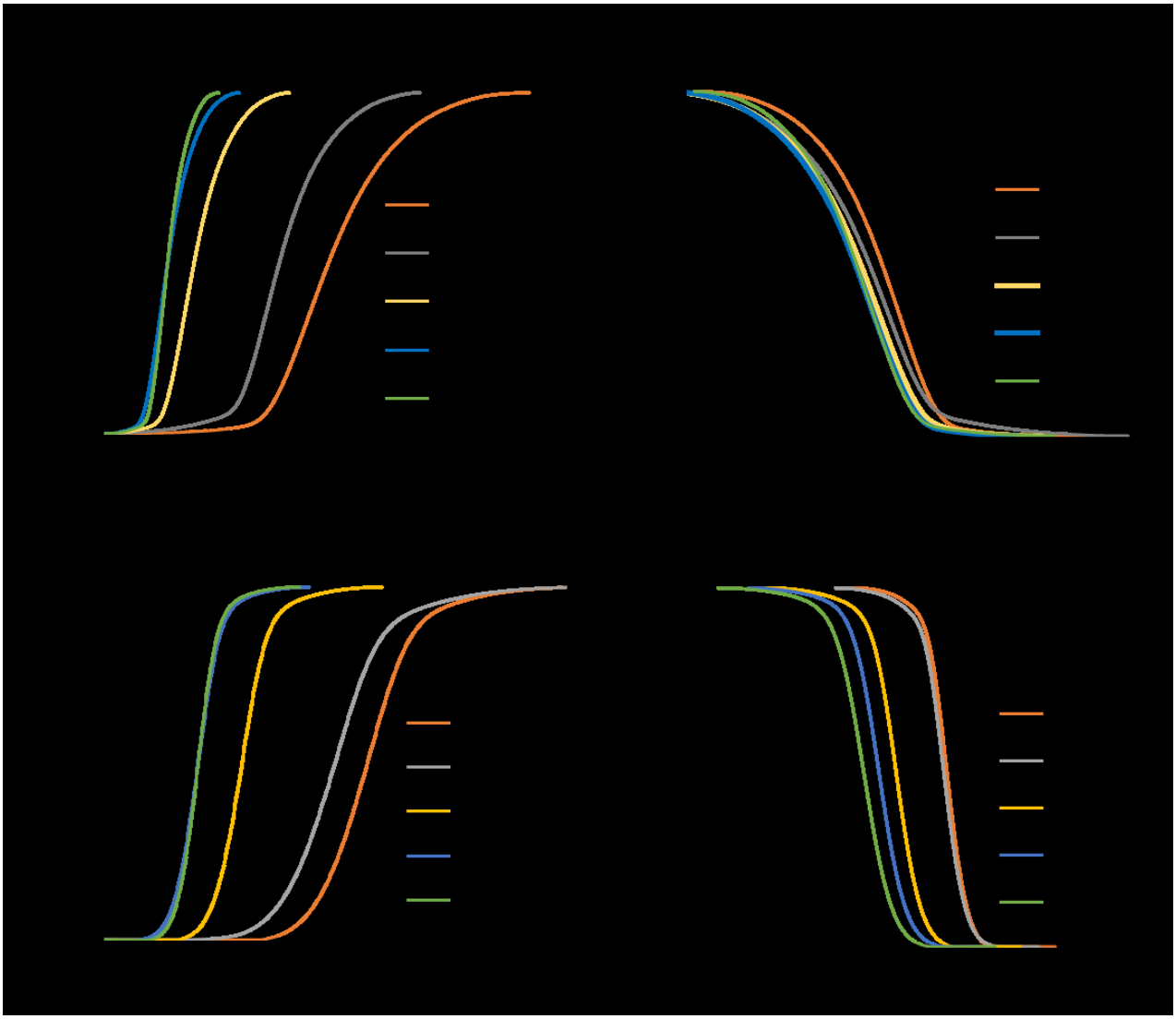

Figure 4. Percent crystallization of a.Technomelt PA 6910 as a function of time; b. Technomelt PA 6910 as a function of temperature; c. PA 6/66 as a function of time; d. PA 6/66 as a function of time, obtained from representative DSC results at different cooling rates.

To define the non-isothermal kinetics of crystallization at constant cooling rates, DSC thermograms at different cooling rates were analyzed by the linearized form of Ozawa's model in Eq. 9.

$$Log(-Ln(1 - x(T))) = Log(k(T)_{oz}) - n\,Log\,r \qquad \text{Eq. 9}$$

The DSC results at constant cooling rates for PA 6/66 and Technomelt PA 6910 were fit to Ozawa's model and are shown in Fig. 5a and Fig. 5b, respectively. The data exhibit good linearity, indicating that Ozawa's theory is valid for both materials. The values for k_{Oz} were derived from Eq. 4 by considering the Ozawa exponent m equal to Avrami's exponent n, which will be derived from isothermal analysis in the next section. For Technomelt PA 6910, n = 1, and for PA 6/66, n = 2. k_{Oz} was also used to calculate the Nakamura rate constant K according to Eq. 6, which is plotted in Fig. 6a as a function of temperature. From Fig. 6, the K values at temperatures close to T_m are lower for Technomelt PA 6910, which indicates slower crystallization of Technomelt PA 6910 at high temperatures. However, Ozawa's theory can only provide information about the kinetics of crystallization at high temperatures close to T_m, and to achieve a full understanding from the kinetics of crystallization of the materials at a wide range of temperatures, isothermal analysis was performed using FSC.

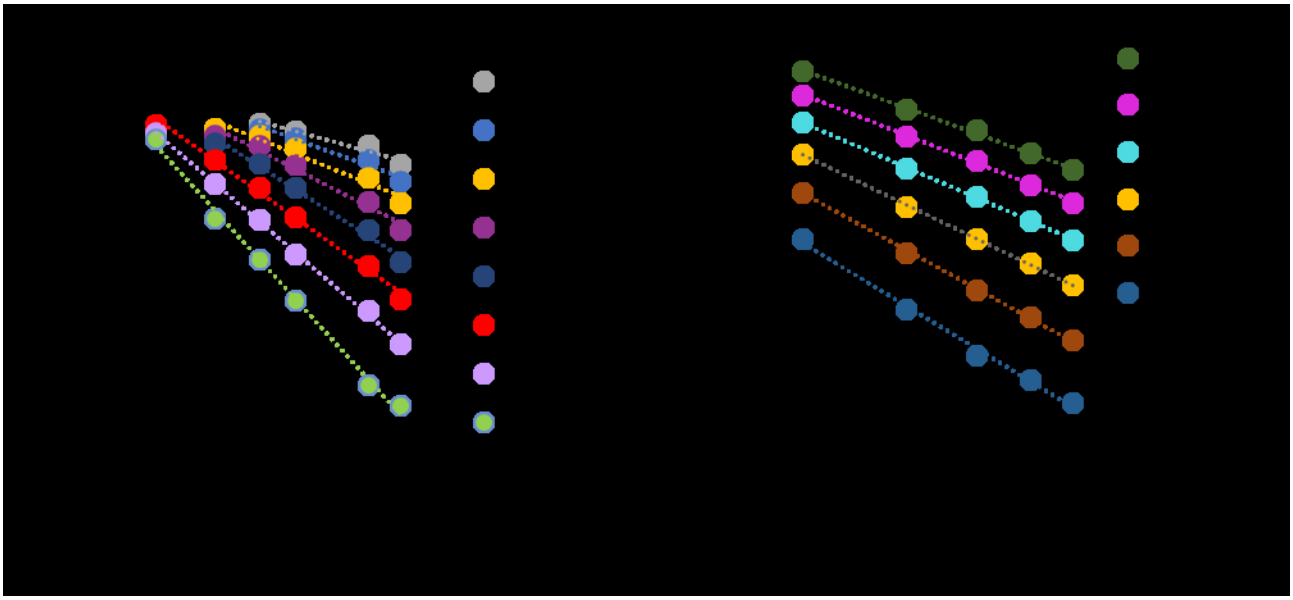

Figure 5. Ozawa plots of log[−ln(1 − X)] versus log r for nonisothermal melt crystallization of (a) PA 6/66 and (b) Technomelt PA 6910.

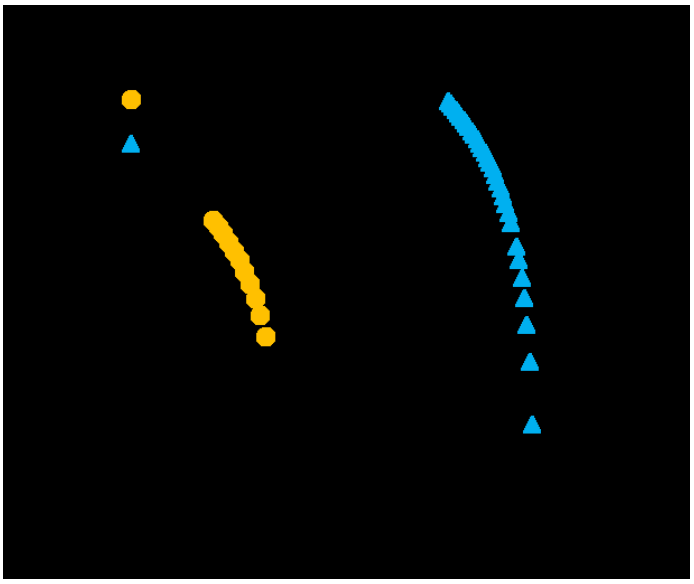

Figure 6. Nakamura constant values as a function of temperature for Technomelt PA 6910 and PA 6/66 obtained from Ozawa model results shown in Figure 5.

Isothermal Analysis

Isothermal analysis proceeded according to the temperature program in Fig. 1b at different annealing times and temperatures. Since the crystallization heat flow during the isothermal step was below the sensitivity of the FSC, a discrete approach was used to define crystallization with respect to time [41]. The discrete method considers ΔH_m after annealing to capture the progress of crystallization with respect to time for a given temperature. Due to the use of fast cooling and heating cycles before and after the isothermal step, molecular reorganization during cooling and cold crystallization during heating is suppressed. Therefore, the measured ΔH_m accounts solely for the fusion of crystallites formed during the annealing step. The results for discrete isothermal analysis at different temperatures in Fig. 7 indicate that the crystallization rates of Technomelt PA 6910 and PA 6/66 are very low at temperatures near T_m with low undercooling, and at temperatures close to T_g with the highest undercooling. Polymers crystallize via nucleation and growth. At low annealing temperatures, nucleation is

thermodynamically favored while the growth of crystallites is suppressed due to the high viscosity of the plastics and restricted diffusion of molecules. This results in slow crystallization and the presence of finely dispersed crystallites within the structure. High temperatures favor the free movement of molecules and the growth of crystallites, while nucleation is the barrier for crystallization due to low undercooling. Therefore, the crystallization rate is low at high temperatures and the morphology develops coarsely and distinctly for higher isothermal holding temperatures [42].

As seen in Fig. 7a, Technomelt PA 6910 crystallizes even at 15 °C, which is above the T_g value of -5 °C obtained by DSC, but below the T_g range of 18 to 30 °C obtained from FSC. The crystallization of PA 6/66 at temperatures below T_g is reported in the literature, in which few of the homogeneous nuclei at the supercooled glass could reach the critical size and were able to grow further into spherulites at long annealing times [43]. As discussed in the previous section, the larger T_g values obtained from FSC are due to the restricted time for relaxation of molecules at high heating rates [38,39]. However, annealing for a long time enables the relaxation of molecules and crystallization at relatively low temperatures.

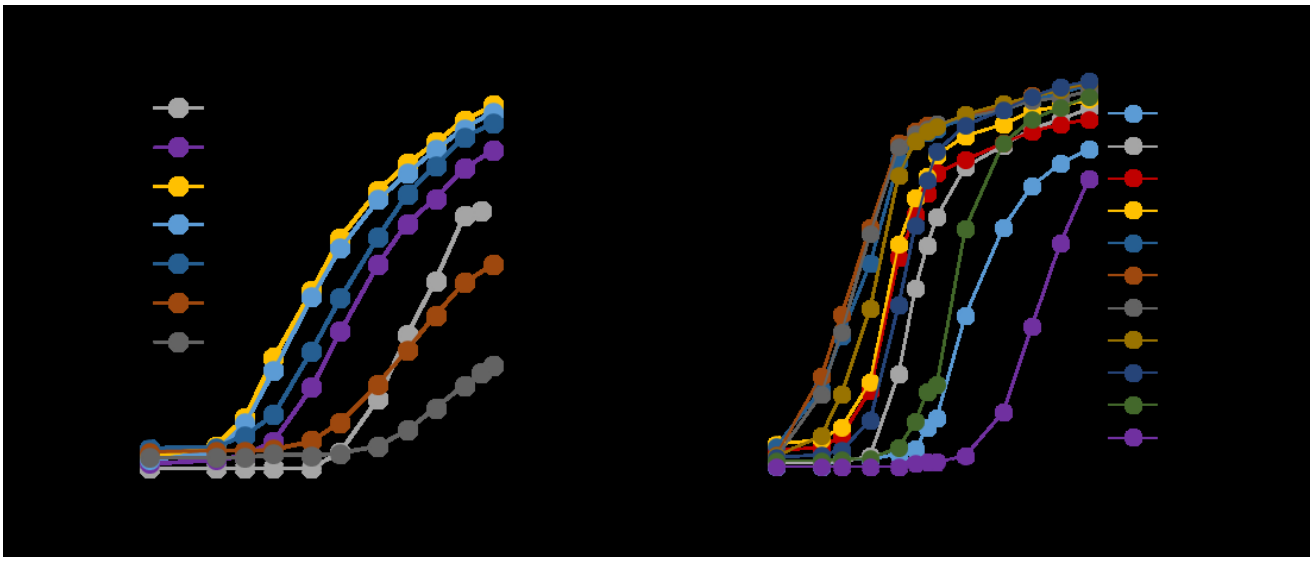

Figure 7. Relative enthalpy of melting after isothermal crystallization as a function of annealing time for a. Technomelt PA 6910; b. PA 6 obtained from FSC results

The half-time crystallization ($t_{0.5}$) values at different annealing temperatures of Technomelt PA 6910 and PA 6/66 are summarized in Fig. 8. The fastest crystallization for Technomelt PA 6910 occurs at 35 °C with $t_{0.5}$ = 35 s, while the shortest $t_{0.5}$ for PA 6/66 is 6 s and was observed at a temperature range of 120 °C to 130 °C. At these temperatures (35 °C for Technomelt PA 6910, and 120 °C-130 °C for PA 6/66), there is a good balance between crystallite nucleation and growth, meaning that the undercooling is sufficiently high to encourage nucleation while the molecules maintain enough mobility for diffusion and crystallite growth. Wang et al. reported that the fastest crystallization for PA 6 occurs at 130 °C with $t_{0.5}$= 1 s, while the fastest crystallization occurred at the temperature range of 120 °C to 130 °C with $t_{0.5}$= 10 s for a copolymer of PA 6 and PA 66 at a molar ratio of 82/18. The reduction in crystallization rate of the copolymer was attributed to the structural mismatching of amide comonomers in hydrogen bonding, which results in restricted mobility within the copolymer. The copolymer of PA 6 and PA 66 in the literature crystallized slightly slower than the PA 6/66 in this study [24].

This difference might be due to the lower content of PA 66 in PA 6/66, which reduces the interactions between different comonomers. These results also suggest that the material used by Wang et al. is closer to the eutectic composition than PA 6/66.

The crystallization half-time curves for both materials are unimodal, implying that there are no significant changes in the nucleation mechanism at different annealing temperatures [19,44]. PA 6 has previously shown a unimodal crystallization half-time curve similar to the PA 6/66 in this study [24,45], while the crystallization half-time curve is bimodal for PA 66 [19,24]. The slower crystallization rate of the PA 6/66 compared to PA 6 and PA 66 implies a random copolymer in which the disrupted chemical periodicity along the chain length results in a lower ability of chains to pack into crystallites [46].

From Fig. 8c, PA 6/66 crystallizes at least five times faster than Technomelt PA 6910. Faster crystallization of PA 6/66 is attributed to the high density of hydrogen bonding, which favors high-temperature crystallization. The hydrogen bonding makes sheet-like structures within the melt. Exposure of the non-hydrogen bonded surface of a sheet-like structure to the melt decreases the required activation energy for crystallization due to its low surface free energy and increases the crystallization rate at high temperatures. Low-temperature crystallization is favored by short-range diffusion of molecules, which requires easy movement of molecules. Therefore, strong hydrogen bonding between the molecules increases the T_g of the material and decreases the crystallization rate at low temperatures [19,24,45].

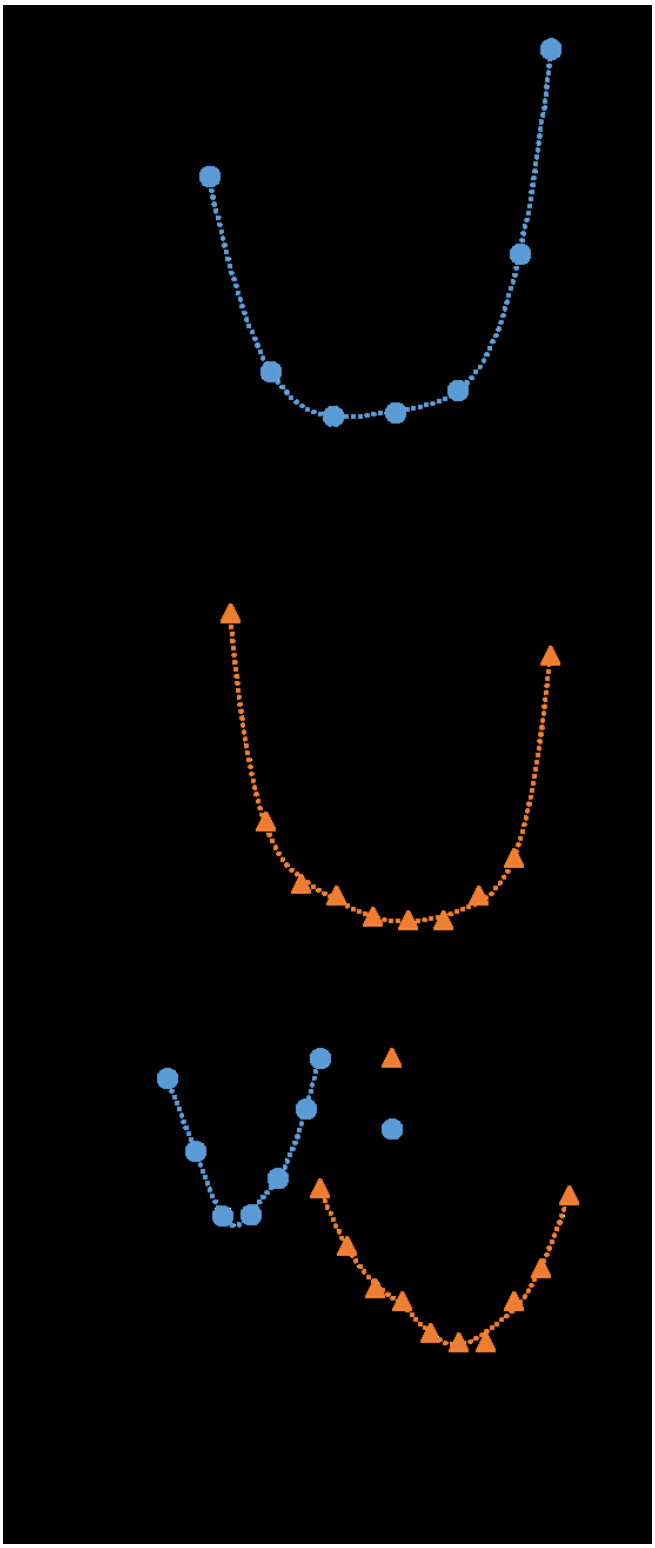

Figure 8. Half-time crystallization of a. Technomelt PA 6910, b. PA 6/66, c. Comparison of both as a function of annealing temperature.

Unlike PA 6/66, which is based on caprolactam with high hydrogen bonding density [47], Technomelt PA 6910 is based on a proprietary blend of dimer fatty acids and diamines. The specific structure of this blend results in the suppression of hydrogen bonding and causes weaker interactions between chains. Lower hydrogen bonding density in the structure accounts for the low T_g and high flexibility of Technomelt PA 6910 as was observed in our previous work [23] and other studies of polyamide-based hot melt adhesives [48–50]. The low density of hydrogen bonding can also reduce the melt viscosity of the material. Lee et al. reported that hydrogen bonding mismatching in the polymer chain of polyamides prevents strong intermolecular bonding and results in lower viscosity [51].

Crystallization of Technomelt PA 6910 continues even at room temperature. The slow crystallization accompanied by ambient temperature crystallization and low melt viscosity likely contribute to Technomelt PA 6910's ability to achieve mechanical properties that are isotropic and comparable to compression molded parts when printed via FFF [23]. FFF-manufactured PA 6 parts revealed inferior and anisotropic mechanical properties [52]. These undesirable properties may result from the high melt viscosity and porous structure of the prints accompanied by the fast crystallization of the PA 6 during printing, which induces large thermomechanical stresses within the parts.

From Fig. 9a, double melting peaks are seen for PA 6/66 at low annealing temperatures. The first melting peak is due to the presence of an unstable γ-phase, and the second melting peak comes from a more stable α-phase. At high annealing times and temperatures, the unstable γ-phases are replaced by more perfect α crystallites and the first melting peak disappears [19]. Fig.

9b indicates that the α-phase is not sensitive to the annealing time and the T_m remains constant implying a perfect crystalline morphology wherein no defects are available to be ameliorated at longer annealing times.

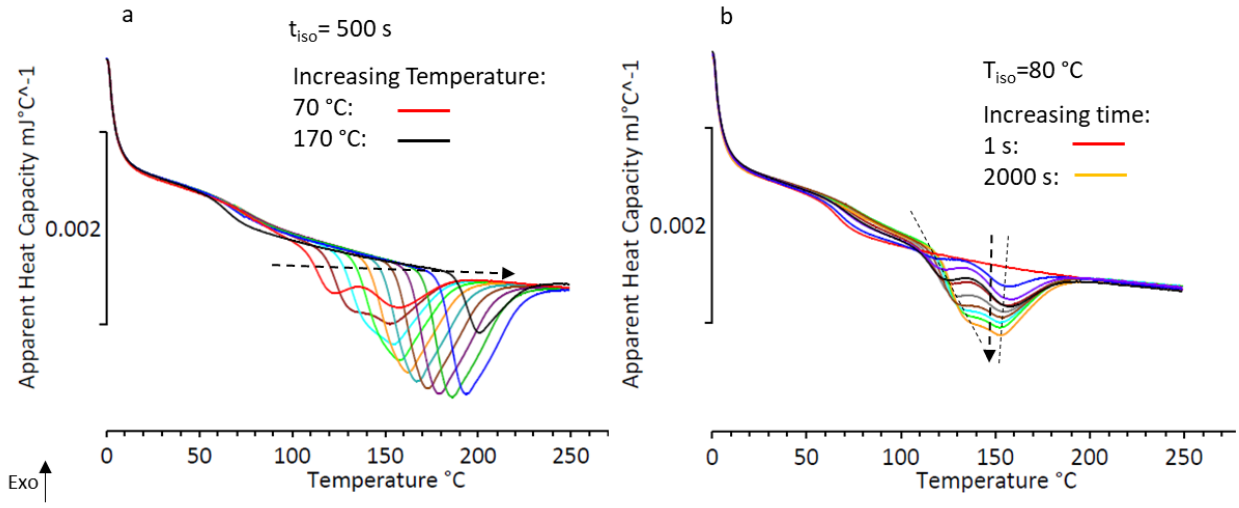

Figure 9. Melting curves of PA 6/66 during the heating cycle after annealing: a. at different temperatures for 500 s; b. at 80 °C for different times. Dashed arrows indicate increasing temperature in a and time in b.

The data from isothermal analysis were fit to the Avrami model (Eq. 1) to determine the n values. The n values for PA 6/66 range from 1.6 to 2.2, which correspond to two-dimensional crystallite growth. The obtained n values from FSC analysis were validated by isothermal DSC analysis at 160 °C and 170 °C. For Technomelt PA 6910, n value range from 0.9 to 1.3, consistent with one-dimensional crystallite growth. Therefore, n=2 for PA 6/66 and n=1 for Technomelt PA 6910 were used for further analyses. The graphs from FSC and DSC analyses to determine the n values are shown in Fig SI. 3.

At x= 50%, the Avrami model simplifies to Eq. 9, and the rate constant k_{Av} was calculated accordingly.

$$k_{Av} = \frac{-Log\ 0.5}{t_{0.5}^{n}} \qquad \text{Eq. 9}$$

The obtained data for k_{Av} were used to determine K using Eq. 6. The K values from isothermal Avrami analysis are plotted in Fig. 10, and compared with the K values from non-isothermal Ozawa analysis. The results indicate a higher K value for PA 6/66, which is in agreement with the half-time crystallization and the DSC analysis by Ozawa's model. The Ozawa analysis provides the K values only at high temperatures. However, there is not a significant difference between the K values obtained from Ozawa and Avrami analysis in Fig. 10, which validates the accuracy of K values obtained from DSC and FSC experiments. The high scan rates in FSC enable accurate kinetic studies at a wide range of temperatures.

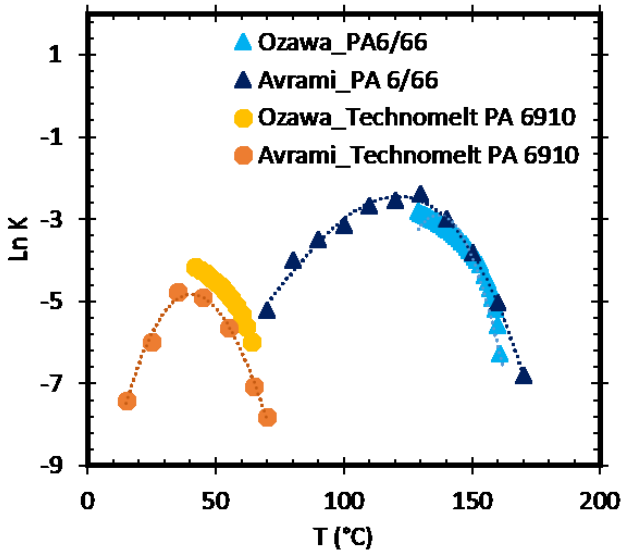

Figure 10. Nakamura constant values as a function of temperature for Technomelt PA 6910 and PA 6/66 obtained from Avrami and Ozawa models.

Conclusion:

In this work, the kinetics of crystallization of two polyamides that are relevant to material extrusion additive manufacturing are compared: a PA 6/66 copolymer and a polyamide-based

hot melt adhesive with the trade name of Technomelt PA 6910. DSC and FSC were used for kinetic studies at non-isothermal and isothermal conditions, respectively. To define the critical cooling rate for isothermal analysis, the heating curves after different cooling rates were studied. These results show that considering the suppression of the melting peak alone is not enough to define the critical cooling rate. To avoid the presence of nuclei in the super-cooled glass at the initial steps of annealing, the cooling rate should be high enough to suppress the relaxation of molecules due to the physical aging and provide a pure amorphous material with a relatively constant T_g.

The kinetic constants obtained from Ozawa's and Avrami's models were used to calculate Nakamura rate constants. There is a good agreement between the K values obtained from both approaches, which further validates the accuracy of the results obtained from FSC and DSC. DSC results provide accurate kinetic data only at high temperatures, while the high scan rates in FSC enable accurate kinetic studies at temperatures between the T_g and T_m of the material. Combining both forms of calorimetry allows for analysis from T_g to well above T_m.

Comparing the kinetic rate constants of two materials, Technomelt PA 6910 crystallizes much slower than PA 6/66. This may be due to the lower density of hydrogen bonding within the structure of Technomelt PA 6910, which suppresses the high-temperature crystallization of the material. The lower hydrogen bonding density results in lower T_g, high flexibility, and low melt viscosity of Technomelt PA 6910. Due to the lower T_g, Technomelt PA 6910 crystallizes at ambient temperature. Crystallization of Technomelt PA 6910 at ambient temperature and its slow crystallization and lower melt viscosity account for the extraordinary mechanical properties of FFF parts in our previous work [23]. PA 6/66 crystallizes rapidly at high temperatures, which

allows for evolution of strength during the rapid cooling of FFF. However, this rapid crystallization can also lead to part warpage. These results encourage the development of new materials for FFF and provide guidance for possible material properties that enable printing of void-free parts with isotropic mechanical properties. Additionally, the obtained Nakamura's kinetic rate constants from this study enable coupling of crystallization kinetics of these materials with thermal models for processing techniques including FFF using the differential form of Nakamura's model, which is a focus of ongoing investigation.

Acknowledgements

The authors acknowledge financial support from the National Science Foundation (CMMI-1853480). The authors also thank the Henkel Corporation for providing Technomelt PA 6910 and Charles Paul, Luca Marchese, and Tim Welters of the Henkel Corporation for insightful conversations and guidance.

References

[1] M. Spoerk, J. Sapkota, G. Weingrill, T. Fischinger, F. Arbeiter, C. Holzer, Shrinkage and Warpage Optimization of Expanded-Perlite-Filled Polypropylene Composites in Extrusion-Based Additive Manufacturing, Macromol. Mater. Eng. (2017). https://doi.org/10.1002/mame.201700143.

[2] J. Tang, B. Xu, Z. Xi, X. Pan, L. Zhao, Controllable Crystallization Behavior of Nylon-6/66 Copolymers Based on Regulating Sequence Distribution, Ind. Eng. Chem. Res. (2018). https://doi.org/10.1021/acs.iecr.8b02671.

[3] X. Zhang, W. Fan, T. Liu, Fused deposition modeling 3D printing of polyamide-based composites and its applications, Compos. Commun. (2020). https://doi.org/10.1016/j.coco.2020.100413.

[4] Y. Jia, H. He, X. Peng, S. Meng, J. Chen, Y. Geng, Preparation of a new filament based on polyamide-6 for three-dimensional printing, Polym. Eng. Sci. (2017). https://doi.org/10.1002/pen.24515.

[5] N. Bachhar, A. Gudadhe, A. Kumar, P. Andrade, G. Kumaraswamy, 3D printing of semicrystalline polypropylene: towards eliminating warpage of printed objects, Bull. Mater. Sci. (2020). https://doi.org/10.1007/s12034-020-02097-4.

[6] C. Hopmann, N. Borchmann, M. Spekowius, M. Weber, M. Schöngart, Simulation of shrinkage and warpage of semi-crystalline thermoplastics, in: AIP Conf. Proc., 2015. https://doi.org/10.1063/1.4918413.

[7] J.M. Fischer, Handbook of Molded Part Shrinkage and Warpage: Second Edition, 2012. https://doi.org/10.1016/C2011-0-06800-X.

[8] M. Pourali, A.M. Peterson, Thermal Modeling of Material Extrusion Additive Manufacturing, in: ACS Symp. Ser., 2019. https://doi.org/10.1021/bk-2019-1315.ch007.

[9] C.G. Schirmeister, T. Hees, E.H. Licht, R. Mülhaupt, 3D printing of high density polyethylene by fused filament fabrication, Addit. Manuf. (2019). https://doi.org/10.1016/j.addma.2019.05.003.

[10] J.N. Hay, P.J. Mills, The use of differential scanning calorimetry to study polymer crystallization kinetics, Polymer (Guildf). (1982). https://doi.org/10.1016/0032-3861(82)90283-X.

[11] Y. Li, L. Duan, L. Cheng, Y. Yang, Y. Li, Y. Cheng, D. Song, Thermal analysis and crystallization kinetics of polyurethane, J. Therm. Anal. Calorim. (2019). https://doi.org/10.1007/s10973-018-7594-z.

[12] R. Le Goff, G. Poutot, D. Delaunay, R. Fulchiron, E. Koscher, Study and modeling of heat transfer during the solidification of semi-crystalline polymers, Int. J. Heat Mass Transf. (2005). https://doi.org/10.1016/j.ijheatmasstransfer.2005.06.015.

[13] M. Zhao, K. Wudy, D. Drummer, Crystallization kinetics of polyamide 12 during Selective laser sintering, Polymers (Basel). (2018). https://doi.org/10.3390/polym10020168.

[14] V. Mathot, M. Pyda, T. Pijpers, G. Vanden Poel, E. Van De Kerkhof, S. Van Herwaarden, F. Van Herwaarden, A. Leenaers, The Flash DSC 1, a power compensation twin-type, chip-based fast scanning calorimeter (FSC): First findings on polymers, Thermochim. Acta. (2011). https://doi.org/10.1016/j.tca.2011.02.031.

[15] R.J. Gaymans, Polyamides, in: Synth. Methods Step-Growth Polym., 1st ed., John Wiley & Sons, 2003: pp. 135–195.

[16] A. Rudin, P. Choi, Introductory Concepts and Definitions, in: Elem. Polym. Sci. Eng., 2013. https://doi.org/10.1016/b978-0-12-382178-2.00001-8.

[17] R.J. Palmer, Polyamides, Plastics, in: Encycl. Polym. Sci. Technol., 2001. https://doi.org/10.1002/0471440264.pst251.

[18] K. Marchildon, Polyamides - Still strong after seventy years, Macromol. React. Eng. (2011). https://doi.org/10.1002/mren.201000017.

[19] X. Li, Y. He, X. Dong, X. Ren, H. Gao, W. Hu, Effects of hydrogen-bonding density on polyamide crystallization kinetics, Polymer (Guildf). (2020). https://doi.org/10.1016/j.polymer.2020.122165.

[20] M. Jin, C. Neuber, H.W. Schmidt, Tailoring polypropylene for extrusion-based additive manufacturing, Addit. Manuf. 33 (2020) 101101. https://doi.org/10.1016/j.addma.2020.101101.

[21] M. Spoerk, C. Savandaiah, F. Arbeiter, J. Sapkota, C. Holzer, Optimization of mechanical properties of glass-spheres-filled polypropylene composites for extrusion-based additive manufacturing, Polym. Compos. (2019). https://doi.org/10.1002/pc.24701.

[22] M. Spoerk, J. Gonzalez-Gutierrez, C. Lichal, H. Cajner, G.R. Berger, S. Schuschnigg, L. Cardon, C. Holzer, Optimisation of the adhesion of polypropylene-based materials during extrusion-based additive manufacturing, Polymers (Basel). (2018). https://doi.org/10.3390/polym10050490.

[23] M. Pourali, A.M. Peterson, Fused filament fabrication of void-free parts using low viscosity hot melt adhesives, Addit. Manuf. (2021). https://doi.org/10.1016/j.addma.2021.102110.

[24] T. Wang, X. Li, R. Luo, Y. He, S. Maeda, Q. Shen, W. Hu, Effects of amide comonomers on polyamide 6 crystallization kinetics, Thermochim. Acta. (2020). https://doi.org/10.1016/j.tca.2020.178667.

[25] M. Avrami, Kinetics of phase change. I: General theory, J. Chem. Phys. (1939). https://doi.org/10.1063/1.1750380.

[26] M. Avrami, Kinetics of phase change. II Transformation-time relations for random distribution of nuclei, J. Chem. Phys. (1940). https://doi.org/10.1063/1.1750631.

[27] M. Avrami, Granulation, phase change, and microstructure kinetics of phase change. III, J. Chem. Phys. (1941). https://doi.org/10.1063/1.1750872.

[28] L. Sangroniz, B. Wang, Y. Su, G. Liu, D. Cavallo, D. Wang, A.J. Müller, Fractionated crystallization in semicrystalline polymers, Prog. Polym. Sci. (2021). https://doi.org/10.1016/j.progpolymsci.2021.101376.

[29] A. Jeziorny, Parameters characterizing the kinetics of the non-isothermal crystallization of poly(ethylene terephthalate) determined by D.S.C., (1978).

[30] S. Vyazovkin, Nonisothermal crystallization of polymers: Getting more out of kinetic analysis of differential scanning calorimetry data, Polym. Cryst. (2018). https://doi.org/10.1002/pcr2.10003.

[31] T. Ozawa, Kinetics of non-isothermal crystallization, Polymer (Guildf). (1971). https://doi.org/10.1016/0032-3861(71)90041-3.

[32] K. Nakamura, T. Watanabe, K. Katayama, T. Amano, Some aspects of nonisothermal crystallization of polymers. I. Relationship between crystallization temperature, crystallinity, and cooling conditions, J. Appl. Polym. Sci. (1972). https://doi.org/10.1002/app.1972.070160503.

[33] R.M. Patel, J.E. Spruiell, Crystallization kinetics during polymer processing—Analysis of available approaches for process modeling, Polym. Eng. Sci. (1991). https://doi.org/10.1002/pen.760311008.

[34] M. Farhoodi, S.M. Mousavi, R. Sotudeh-Gharebagh, Z. Emam-Djomeh, A. Oromiehie, H. Mansour, A study on physical aging of semicrystalline polyethylene terephthalate below the glass transition point, J. Appl. Res. Technol. (2012). https://doi.org/10.22201/icat.16656423.2012.10.5.360.

[35] I. Kolesov, R. Androsch, The rigid amorphous fraction of cold-crystallized polyamide 6, Polymer (Guildf). (2012). https://doi.org/10.1016/j.polymer.2012.08.017.

[36] N. Yaghini, G.W.M. Peters, Modeling Crystallization Kinetics and Resulting Properties of Polyamide 6, Macromolecules. (2021). https://doi.org/10.1021/acs.macromol.0c02588.

[37] J.E.K. Schawe, Influence of processing conditions on polymer crystallization measured by fast scanning DSC, in: J. Therm. Anal. Calorim., 2014. https://doi.org/10.1007/s10973-013-3563-8.

[38] C.T. Moynihan, A.J. Easteal, J. Wilder, J. Tucker, Dependence of the glass transition temperature on heating and cooling rate, J. Phys. Chem. (1974).

https://doi.org/10.1021/j100619a008.

[39] R. Brüning, K. Samwer, Glass transition on long time scales, Phys. Rev. B. (1992). https://doi.org/10.1103/PhysRevB.46.11318.

[40] J.E.K. Schawe, Measurement of the thermal glass transition of polystyrene in a cooling rate range of more than six decades, Thermochim. Acta. (2015). https://doi.org/10.1016/j.tca.2014.05.025.

[41] X. Tardif, B. Pignon, N. Boyard, J.W.P. Schmelzer, V. Sobotka, D. Delaunay, C. Schick, Experimental study of crystallization of PolyEtherEtherKetone (PEEK) over a large temperature range using a nano-calorimeter, Polym. Test. (2014). https://doi.org/10.1016/j.polymertesting.2014.03.013.

[42] C. Fischer, D. Drummer, Crystallization and Mechanical Properties of Polypropylene under Processing-Relevant Cooling Conditions with respect to Isothermal Holding Time, Int. J. Polym. Sci. (2016). https://doi.org/10.1155/2016/5450708.

[43] R. Androsch, C. Schick, J.W.P. Schmelzer, Sequence of enthalpy relaxation, homogeneous crystal nucleation and crystal growth in glassy polyamide 6, Eur. Polym. J. (2014). https://doi.org/10.1016/j.eurpolymj.2014.01.012.

[44] F. Paolucci, D. Baeten, P.C. Roozemond, B. Goderis, G.W.M. Peters, Quantification of isothermal crystallization of polyamide 12: Modelling of crystallization kinetics and phase composition, Polymer (Guildf). (2018). https://doi.org/10.1016/j.polymer.2018.09.037.

[45] Y. He, R. Luo, Z. Li, R. Lv, D. Zhou, S. Lim, X. Ren, H. Gao, W. Hu, Comparing Crystallization Kinetics between Polyamide 6 and Polyketone via Chip-Calorimeter Measurement, Macromol. Chem. Phys. (2018). https://doi.org/10.1002/macp.201700385.

[46] A.H. WINDLE, A METALLURGIST'S GUIDE TO POLYMERS, in: Phys. Metall., 1996. https://doi.org/10.1016/b978-044489875-3/50037-5.

[47] V. Moody, H.L. Needles, Major Fibers and Their Properties, in: Tufted Carpet, 2004. https://doi.org/10.1016/b978-188420799-0.50004-x.

[48] P.G. Kadam, S.T. Mhaske, Synthesis and properties of polyamide derived from piperazine and lower purity dimer acid as hot melt adhesive, Int. J. Adhes. Adhes. (2011). https://doi.org/10.1016/j.ijadhadh.2011.06.019.

[49] X. Chen, H. Zhong, L. Jia, J. Ning, R. Tang, J. Qiao, Z. Zhang, Polyamides derived from piperazine and used for hot-melt adhesives: Synthesis and properties, Int. J. Adhes. Adhes. (2002). https://doi.org/10.1016/S0143-7496(01)00039-2.

[50] R.F.R. Freitas, C. Klein, M.P. Pereira, R.B. Duczinski, S. Einloft, M. Seferin, R. Ligabue, Lower purity dimer acid based polyamides used as hot melt adhesives: Synthesis and properties, J. Adhes. Sci. Technol. (2015). https://doi.org/10.1080/01694243.2014.1001961.

[51] J. Lee, W.G. Seo, J. Kim, Y.S. Kim, Y. Yoo, J.H. Moon, S.G. Kim, H.M. Jung, Amide-based oligomers for low-viscosity composites of polyamide 66, Macromol. Res. (2017). https://doi.org/10.1007/s13233-017-5129-2.

[52] S. Terekhina, T. Tarasova, S. Egorov, I. Skornyakov, L. Guillaumat, M.L. Hattali, The effect of build orientation on both flexural quasi-static and fatigue behaviours of filament deposited PA6 polymer, Int. J. Fatigue. (2020). https://doi.org/10.1016/j.ijfatigue.2020.105825.